University of Wollongong
Research Online

Australian Institute for Innovative Materials - Papers

Australian Institute for Innovative Materials

2010

Intergrain connectivity of MgB2 ceramics studied by impedance analysis

C.C Wang
ISEM

C Wang
Chinese Academy of Sciences

Rong Zeng
University of Wollongong, rzeng@uow.edu.au

S X. Dou
University of Wollongong, shi@uow.edu.au

Publication Details

Wang, CC, Wang, C, Zeng, R & Dou, SX (2010), Intergrain connectivity of MgB_2 ceramics studied by impedance analysis, Journal of Applied Physics, 108(2), pp. 023901-1-023901-6.

Research Online is the open access institutional repository for the University of Wollongong. For further information contact the UOW Library: research-pubs@uow.edu.au

Intergrain connectivity of MgB2 ceramics studied by impedance analysis

Abstract

First, by using of the conventional Rowell analysis, we demonstrated that the addition of nano BN particles can effectively eliminate MgO and pores in MgB_2 resulting in a very high density and good connectivity of BN-doped MgB2. Then, another method—low-frequency dielectric impedance analysis—was introduced to characterize the properties of the grain boundaries of MgB_2. A comparative impedance study was performed in the frequency range from 100 Hz to 100 MHz on pure and nano BN-doped MgB_2. The study revealed some following interesting results: (1) a dielectric resonance around frequency of 10^8 in both samples was observed, which was argued to be related to an inductance-capacitance and (2) the pure sample has two dielectric relaxations originating from intergrains, while the doped sample has only one intergranular contribution. This convinces that the electric connectivity of the doped sample is really improved by the addition of nano BN particles. Our results indicate that dielectric technique may be a useful tool to characterize the grain boundary properties and grain boundary-related properties of MgB_2.

Keywords

Intergrain, connectivity, MgB2, ceramics, studied, impedance, analysis

Disciplines

Engineering | Physical Sciences and Mathematics

Publication Details

Wang, CC, Wang, C, Zeng, R & Dou, SX (2010), Intergrain connectivity of MgB_2 ceramics studied by impedance analysis, Journal of Applied Physics, 108(2), pp. 023901-1-023901-6.

This journal article is available at Research Online: http://ro.uow.edu.au/aiimpapers/202

Intergrain connectivity of MgB_2 ceramics studied by impedance analysis

C. C. Wang,[1,2,a)] C. Wang,[3] R. Zeng,[1] and S. X. Dou[1]
[1]*Institute of Superconducting and Electronic Materials, Wollongong University, Northfield Ave, Gwynneville, New South Wales 2522, Australia*
[2]*Laboratory of Dielectric Functional Materials, School of Physics and Material Science, Anhui University, Hefei 230039, China*
[3]*Institute of Physics and Center for Condensed Matter Physics, Chinese Academy of Sciences, Beijing 100190, People's Republic of China*

(Received 6 April 2010; accepted 9 June 2010; published online 16 July 2010)

First, by using of the conventional Rowell analysis, we demonstrated that the addition of nano BN particles can effectively eliminate MgO and pores in MgB_2 resulting in a very high density and good connectivity of BN-doped MgB_2. Then, another method—low-frequency dielectric impedance analysis—was introduced to characterize the properties of the grain boundaries of MgB_2. A comparative impedance study was performed in the frequency range from 100 Hz to 100 MHz on pure and nano BN-doped MgB_2. The study revealed some following interesting results: (1) a dielectric resonance around frequency of 10^8 in both samples was observed, which was argued to be related to an inductance-capacitance and (2) the pure sample has two dielectric relaxations originating from intergrains, while the doped sample has only one intergranular contribution. This convinces that the electric connectivity of the doped sample is really improved by the addition of nano BN particles. Our results indicate that dielectric technique may be a useful tool to characterize the grain boundary properties and grain boundary-related properties of MgB_2. © *2010 American Institute of Physics*. [doi:10.1063/1.3462398]

I. INTRODUCTION

The binary metallic MgB_2 superconductor with extremely high transition temperature close to 40 K,[1] several times higher than those of conventional metallic superconductors, holds tremendous promise for a wide range of large-scale applications, especially for next generation superconducting magnets operating at around 20 K without cryogen.[2] However, the strong field-dependent critical current density (J_C) represents one of the main stumbling blocks in realizing this potential application. It is clear that J_C is determined not only by the electrical intergrain connectivity, but also by the flux pinning strength of the grain boundaries. Some impurity phases such as pores, MgO, boron oxide, and other precipitates make the grain boundaries very blocked, thereby largely reducing the effective cross-sectional area of the sample and in turn decreasing the J_C. Enormous efforts focusing on reducing and eliminating the poor electrical connectivity have been widely attempted in recent years (see recent review articles in Refs. 3–5, and references therein). On the other hand, in order to appreciate the connectivity, Rowell *et al.*[6,7] suggested that the normal-state resistivity can be used as a gauge of connectivity. They even derived a finitely relationship $J_C \propto 1/\Delta\rho_{300-50\ \mathrm{K}}$($\Delta\rho_{300-50\ \mathrm{K}}$ is the resistivity difference between 300 and 50 K) in epitaxial thin film system.[7] Yamamoto *et al.*[8] and Eisterer *et al.*[9] modeled the reduced effective cross section (connectivity) in terms of percolation method. Their results indicate that the low packing factor and poor connectivity strongly restrict J_C in MgB_2. Many experimental methods, such as Campbell's method,[10] magneto-optical and electromagnetic studies,[11] magnetoresistance and radio frequency penetration depth techniques[12] have been used to investigate the intergrain connectivity of MgB_2.

It is well known that dielectric technique, especially the impedance spectrum, can provide relevant information about the grain boundary. This technique has been proved to be a sensitive probe to detect the electron behavior in strongly electron-correlated high-temperature superconducting cuprate systems.[13,14] It is, therefore, expected that the dielectric investigations of MgB_2 may shed some lights on the intergrain properties. Unfortunately, most of the existing reports on dielectric properties of MgB_2 were measured on microwave and optical frequency range.[15–18] In such a high-frequency range, the dielectric polarization of the grain boundary known as interface polarization cannot follow the variations in the applied field and hence the intergrain properties cannot be characterized by these measurements. Herein, we present results of low-frequency (10^2 to 10^8 Hz) impedance analysis for both pure and nano BN (hexagonal, *h*-BN) doped MgB_2 ceramics. The *h*-BN addition was chosen because it is a structural analog of carbon which has been proved to be an effective dopant in improving the J_C.[19] The results reveal that BN-doping can effectively improve the connectivity and suggest that the impedance spectra may be a useful tool to investigate the connectivity of MgB_2 ceramics.

II. EXPERIMENTAL DETAILS

Samples were fabricated by a diffusion reaction method. Starting powder of crystalline B with the purity of 99.999% with and without 10 wt % BN (with an average particle size of 500 nm) were thoroughly mixed and pressed into pellets.

[a)]Electronic mail: ccwang@ahu.edu.cn.

 © 2010 American Institute of Physics

Downloaded 16 Aug 2012 to 130.130.37.84. Redistribution subject to AIP license or copyright; see http://jap.aip.org/about/rights_and_permissions

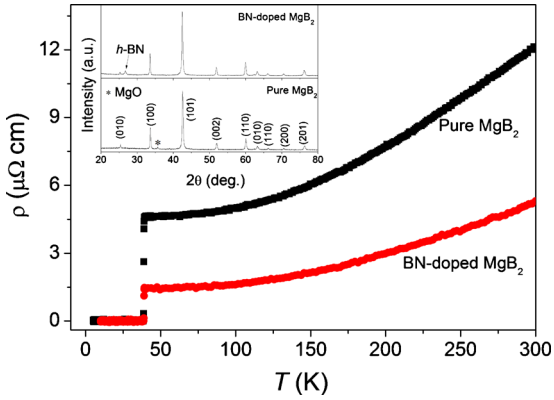

FIG. 1. (Color online) Resistivity as a function of temperature for pure and BN-doped samples. Inset shows the XRD patterns of both samples.

The pellets were then sealed into an iron tube filled with Mg powder (99.8%) with the nominal composition ratio of Mg:B=1.15:2.0. Finally, the ion tube was sintered at 850 °C for 10 h in a quartz tube furnace and then cooled down to room temperature. A high-purity Ar gas flow was maintained throughout the sintering process. All samples were characterized by x-ray diffraction (XRD) using a Philips diffractometer with Cu $K\alpha$ radiation. Dielectric measurements were carried out at room temperature using an Agilent 4294 A impedance analyzer. Silver paste was used for top and bottom electrodes. The ac measuring signal was 100 mV_{rms}. Magnetic properties were measured using a physical properties measurement system (PPMS, Quantum Design). The Bean model[20] was used to calculate the magnetic critical current density. The magnetoresistivity, $\rho(H,T)$, was measured by using the four probe method with the magnetic field H applied perpendicular to the current direction. The upper (H_{C2}) and irreversible (H_{irr}) critical fields were determined as the 90% and 10% transition on the $\rho(H,T)$ curves, respectively.

III. RESULTS AND DISCUSSIONS

A. General properties

Figure 1 shows the XRD patterns and temperature-dependent resistivity of the pure and BN-doped MgB_2. Both samples show virtually identical lattice parameters and same superconducting transition temperature (T_C) as summarized in Table I. From Fig. 1 and Table I, following three notable features can be extracted: (1) no evident MgO was detected by XRD in the doped sample indicating the impurity phase of MgO can be greatly eliminated by the addition of nano h-BN. Since MgO was proved to be an important current barrier in MgB_2, the elimination of MgO results in largely decrease in resistivity as illustrated in the main panel; (2) the doped sample exhibits very higher density (nearly 90% of the theoretical density); and (3) following the Rowell analysis,[7] a constant $\Delta\rho_{ideal}$ of 7.3 $\mu\Omega$ cm for fully connected sample[21] was adopted to scale the total cross-sectional area (A_F) which was found to be 97% for the pure sample and 188% for the BN-doped. The value of A_F larger than 100% indicates that the Rowell analysis derived from film system may not quantitatively hold true for ceramic system. However, it qualitatively indicates that the doping of nano h-BN can significantly improve the connectivity. This feature may be because that h-BN is a good lubricant additive which can be perfectly mixed with both ceramics and alloys and as a consequence it drastically reduces the volume fraction of pore in the doped sample leading to high density as already seen in feature (2). However, a controversial result, i.e., a substantially decreased J_C was reported by Kováč *et al.*[22] in 10 wt % BN-doped MgB_2 sintered at 950 °C for half an hour. This negative effect might be because that the sintering time of their sample is so short that the BN particles only act as impurities, which reduce the connectivity. Whereas our sample made by diffusion method sintering at high temperature for a long time (10 h), the h-BN particles act as a good lubricant and the MgB_2 grains have enough time to adjust their positions leading to the elimination of the pores and thus a good connectivity.

The improved connectivity of the doped sample can be demonstrated by the properties of J_C. Figure 2(a) shows the magnetic J_C versus field at 5 and 20 K for the pure and doped samples. It is clearly seen that the h-BN addition has obviously improved the in-field J_C properties. For example, the doped sample shows a J_C of 6444 A/cm^2 at 20 K and 4 T, at temperatures and fields interest for application. This value is almost four times larger than that of the pristine sample. Figure 2(b) presents the H_{C2} and H_{irr} as functions of the temperature for the pure and doped samples. As can be seen, both samples have no significant deference in H_{C2} and H_{irr}, indicating that the addition of h-BN is primarily affecting the connectivity, rather than enhancing the pinning strength that causes notable enhancement of H_{irr}.[23] This result is further supported by the field dependence of the volume pinning force $F_p(H)$ at 20 K shown in Fig. 2(c), therein, $F_p(H)$ is normalized by the maximum volume pinning force $F_{p\,Max}$. The $F_p/F_{p\,Max}$ curve of the doped sample shifts slightly to high field than that of the pure sample indicating a marginal enhanced pinning force. Thus, we can come to the conclusion that the doping of h-BN can significantly improve the connectivity of MgB_2. Finally, it is worth noting that J_C is enhanced notably in high-field range due to the improved connectivity, but no significant enhancement is observed at low fields. This might be because that J_C is mainly determined by connectivity and disorder. The latter enhances J_C

TABLE I. Summaries of characteristic data for the pure and BN-doped samples.

Sample	Density (g/cm^3)	a (Å)	c (Å)	c/a	T_C (K)	RRR	$\Delta\rho_{300-40\ K}$ ($\mu\Omega$ cm)	A_F (%)
Pure MgB_2	1.86	3.085	3.523	1.141	38.8	2.64	7.53	97
BN-doped MgB_2	2.15	3.082	3.521	1.141	38.8	3.76	3.89	188

Downloaded 16 Aug 2012 to 130.130.37.84. Redistribution subject to AIP license or copyright; see http://jap.aip.org/about/rights_and_permissions

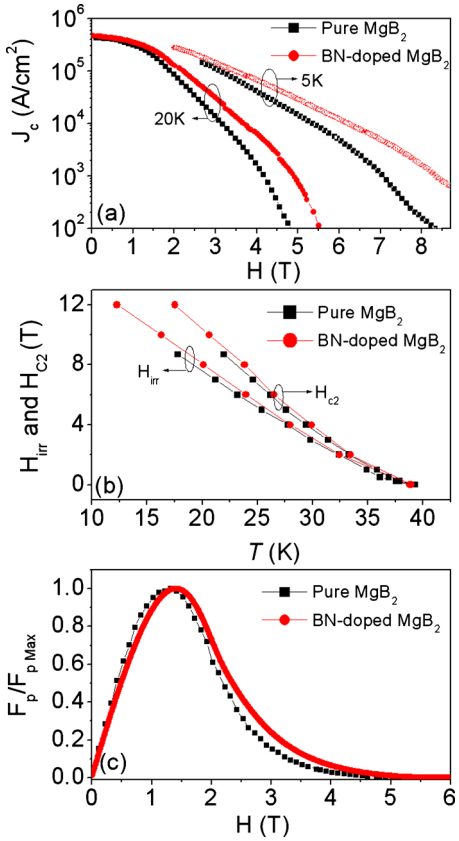

FIG. 2. (Color online) (a) Critical current density, J_C, as a function of magnetic field at 5 and 20 K for pure and BN-doped samples. (b) Temperature dependence of H_{C2} and H_{irr} for both samples. (c) Field dependence of the normalized pinning force at 20 K for both samples.

remarkably at low fields because all the defects such as MgO particles and pores act as pinning centers. When these defects were effectively eliminated, it will produce a negative influence on J_C. The measured J_C at low-field range is a compromise between the positive effect caused by the improved connectivity and the negative effect due to the lack of enough pinning centers. The tiny enhancement of J_C in the doped sample indicating that the positive effect of connectivity on J_C is more important than the negative effect of disorder.

B. Impedance analysis

To further substantiate the above conclusion, we performed detailed impedance analysis for both samples. Figure 3 shows the real (C') and imaginary (C'') parts of the capacitance as a function of frequency for the pure and BN-doped samples. Similar dielectric properties for both samples can be seen. A salient feature of the real part is that both samples exhibit a dielectric resonance around 10^8 Hz. Generally, a dielectric resonance can be observed in infrared frequency range (10^{12} Hz) where the bonding electrons (or ions) respond to the variations in the applied field in the form of harmonic oscillation. In La_2CuO_4 single crystal, a dielectric resonance occurring at approximately gigahertz was ascribed to the harmonic oscillation of extremely massive ($1100m_e$, with m_e the mass of free electron) charge carriers.[24] However, the effective mass of carries in MgB_2 was found to

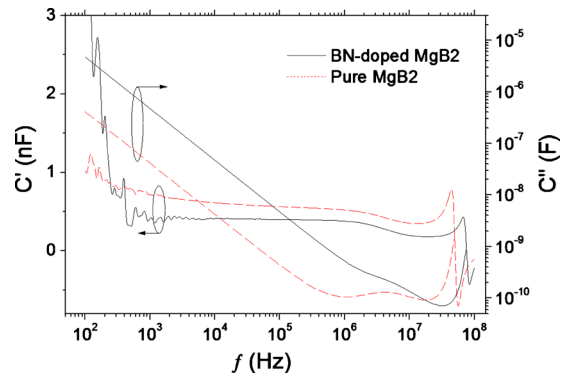

FIG. 3. (Color online) Frequency dependence of the real (C') and imaginary (C'') parts of the complex capacitance for pure and BN-doped MgB_2.

range from 0.44 to $0.68m_e$.[25] This fact suggests that a mechanism other than the harmonic oscillation of confined carriers underlies the observed resonance. From the imaginary part, three features can be seen for both samples: a linear part below 10^6 Hz, a hump around 10^7 Hz, and a peak (not fully detected) corresponding to the resonance at the highest frequencies. The linear part agrees very well with previous report of low-frequency dielectric study.[26] This part shows a perfect slope of -1, which is the typical reciprocal frequency behavior that implies the system displays nondispersive transport of free charge carriers. This result strongly supports the fact that the normal-state resistivity of MgB_2 is determined by electron–phonon interaction and can be well described by Bloch–Grüneisen formula. The hump indicates the existence of a dielectric relaxation in the tested samples.

We now turn our attention to the origin of the resonance and the relaxation. First, we focus our discussion on the BN-doped sample, then a comparison between the pure and doped samples will be given late to show that the improved connectivity for the doped sample. A conceivable origin of the observed resonance is the inductance-capacitance (LC) resonance, since the sample exhibits good conductivity as seen in Fig. 1, the inductive effect of the measuring system may become evident. To find out whether or not the observed resonance is related to LC resonance, we performed impedance measurements under different dc biases (V).

Figure 4 is the complex impedance plot (Z'' versus Z'). Apart from the upturn at the highest frequencies due to the resonance, a semicircular arc can be seen. The resonant part separates well from the arc part with a demarking frequency f_d found to decrease with biases. For example, f_d is 7.59×10^7 Hz for $V=0$ V, which decreases to 5.01×10^7 Hz for $V=1.0$ V. Theoretically, the grains, grain boundaries, and electrode-sample contacts can make contributions to the arc. The arc can be greatly depressed by the applied biases, indicating its extrinsic nature from the grain boundaries and/or contacts.[27] To further distinguish the grain boundary and contact contributions, we replot the same data in Fig. 4 in an alternative presentation of Z' versus Z''/f in Fig. 5. In this kind of presentation, three sectional straight lines (or nearly straight lines) can usually be obtained with the sequential regions from low to high frequencies corresponding, respectively, to the dielectric response from the contacts, grain boundaries, and bulk grains.[28,29] The slope of the lines rep-

Downloaded 16 Aug 2012 to 130.130.37.84. Redistribution subject to AIP license or copyright; see http://jap.aip.org/about/rights_and_permissions

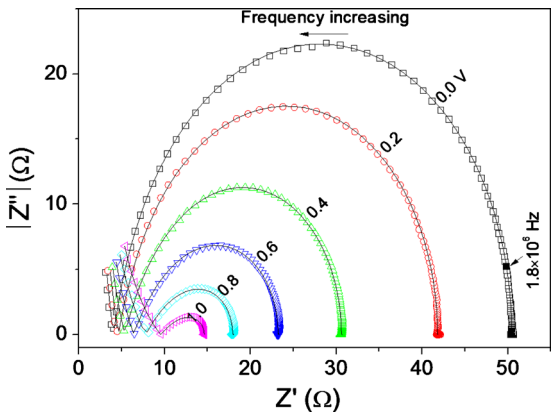

FIG. 4. (Color online) Complex impedance spectra of BN-doped MgB_2 at different dc biases. The open symbols are experimental data, the solid curves are fitting results based on the equivalent circuit shown as an inset in Fig. 5. The arrow points to the closed square that indicates the critical frequency where the polarization changes from the electrode type to the grain boundary type.

resents the eigenfrequency of the corresponding dielectric responses. From Fig. 5 only two sectional linear lines for each curve can be seen, which indicates that only the dielectric responses from contacts and grain boundaries can be detected. These two dielectric responses separate well from each other with a critical frequency found to increase from 1.80×10^6 Hz for $V=0$ V to 3.39×10^6 Hz for $V=1.0$ V. Based on the value of the critical frequency, it was found that the contact response has negligible contribution to the observed semicircular arc. Taking the curve of $V=0.0$ V as an example, the critical frequency indicated by a closed square and an arrow locates very closely to the commence point of the arc (see Fig. 4). Therefore, the measured relaxation belongs entirely to the grain boundaries. More interestingly, as representatively indicated by an arrow in Fig. 5 on the curve of $V=0.0$ V, the data points of the resonant part starting from f_d shown as closed squares fall perfectly on the same line holding by the grain boundary relaxation. This implies that the dielectric resonance is intimately related to the relaxation, which can be well understood based on the same equivalent circuit as shown by the inset of Fig. 5. The circuit

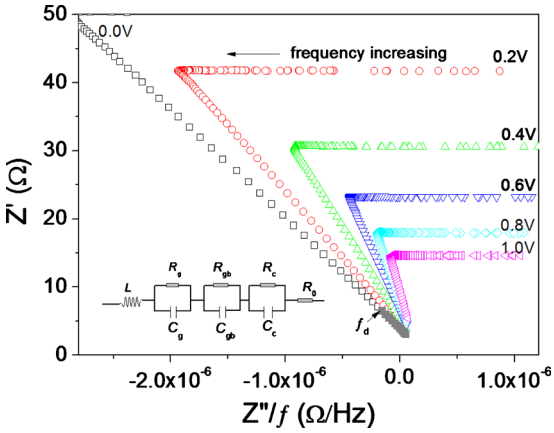

FIG. 5. (Color online) Replots the complex impedance spectra in Fig. 4 using the presentation of Z' vs Z''/f. The closed squares denote that these data are related to the resonance. Inset shows the equivalent circuit.

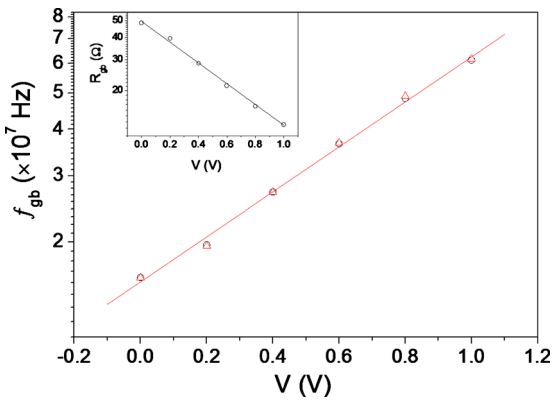

FIG. 6. (Color online) Bias-dependence of the eigenfrequency of the grain boundary (f_{gb}) obtained from the experiments (open circles) and fittings (open triangles). Inset shows the bias-dependence of the resultant grain boundary resistance. The straight lines are the linear fitting results.

consists an inductance and an uncompensated resistance (R_0) in series with three serially connected RC (R=resistance, C=capacitance) units representing the grains, grain boundaries, and contacts. The real and imaginary parts of the complex impedance ($Z^*=Z'+jZ''$) obtained from the circuit are:

$$Z' = R_0 + R_g/[1+(f/f_g)^2] + R_{gb}/[1+(f/f_{gb})^2] + R_c/[1+(f/f_c)^2], \quad (1)$$

$$Z'' = -R_g(f/f_g)/[1+(f/f_g)^2] - R_{gb}(f/f_{gb})/[1+(f/f_{gb})^2] - R_c(f/f_c)/[1+(f/f_c)^2] + fL, \quad (2)$$

where f is the frequency, j is the square root of -1, the subscripts g, gb, and c denote the grains, grain boundaries, and contacts, respectively, and $f_i=1/(R_iC_i)$ $(i=g,gb,c)$ is the eigenfrequency. The eigenfrequency (i.e., the slope of the linear line in Fig. 5) of the contacts and grain boundaries were found to be at the magnitude of 10^2–10^3 Hz and 10^7 Hz, respectively. As already mentioned that the sample shows good dc conductivity, which implies the grain resistivity is very small. The absence of dielectric response of the grains as revealed by Fig. 5 indicates that the eigenfrequency of the grain is so high that it is far out of the measuring frequency window. In the frequency range around 10^7 Hz, we therefore have $f_c \ll f \ll f_g$, then Eqs. (3) and (4) can be rewritten as:

$$Z' = R_0 + R_g + R_{gb}/[1+(f/f_{gb})^2], \quad (3)$$

$$Z'' = -R_{gb}(f/f_{gb})/[1+(f/f_{gb})^2] + fL. \quad (4)$$

Combining Eqs. (3) and (4), one obtains

$$Z' = R_0 + R_g + f_{gb}L - f_{gb}(Z''/f). \quad (5)$$

Obviously, in the frequency range where the grain boundaries and resonance contributions predominate, the presentation of Z' versus Z''/f exhibits a straight line with the common slope of $-f_{gb}$ for both grain boundary relaxation and resonance. This result clearly confirms the LC mechanism of the resonance. It is interesting to note that an exponential increase in f_{gb}, as shown by open circles in Fig. 6, is found in the investigated bias range. This fact implies that R_{gb} should

Downloaded 16 Aug 2012 to 130.130.37.84. Redistribution subject to AIP license or copyright; see http://jap.aip.org/about/rights_and_permissions

TABLE II. Parameters obtained from the least-squares fittings for impedance spectrum of BN-doped sample based on the equivalent circuit.

Bias (V)	R_0 (Ω)	R_{gb} (Ω)	R_c (Ω)	C_{gb} (nF)	C_c (F)	L (nH)
0	2.08	48.38	0.09	1.29	0.18	122.47
0.2	2.23	39.57	0.05	1.30	0.05	122.44
0.4	2.02	28.58	0.07	1.29	0.01	123.39
0.6	1.85	21.39	0.12	1.28	0.002	124.88
0.8	1.64	16.30	0.09	1.25	0.002	125.95
1.0	1.82	12.80	0.06	1.27	0.003	125.32

exponentially decrease with increasing biases, since $f_{gb} = 1/(R_{gb}C_{gb})$, where C_{gb} depends on the geometric configuration and can be treated as bias-independent. The bias-dependent grain boundary resistance has been reported by several authors,[30,31] there, the grain boundary conductivity obeys the "field activated" Arrhenius law $\sigma_{gb}=\sigma_0 \exp(-E/k_BT)$, ($\sigma_0$ is the pre-exponential factor,k_B is the Boltzmann constant, and E is the activation energy or potential barrier) with the bias-dependent activation energy $E=E_0-\alpha V$ (E_0 is the activation energy at $V=0$, α is a constant). The present results agree very well with this Arrhenius behavior, substantially convincing that the observed dielectric relaxation is due to the contribution of the grain boundaries. On the other hand, the impedance spectrum can be well fitted based on the equivalent circuit. The fitting results displayed as solid curves in Fig. 4 agree perfectly with the experimental data. The resultant parameters are listed in Table II, about which following two points are worth noting: (1) Despite the notable uncertainty of the resultant parameters R_c and C_c due to the large uncertainty of the data points in the low-frequency range below 1 MHz, the $1/(R_cC_c)$ at various biases yields the eigenfrequency of the contact of the same order (10^2–10^3 Hz) with that deduced from Fig. 5. (2) The resultant parameter of C_{gb} truly keeps as a constant within the fitting uncertainty, and R_{gb} is found to decrease exponentially with increasing bias as shown in the inset of Fig. 6, from which the E_0 and α are deduced to be 105 meV and 35 meV/V, respectively. The values of f_{gb} obtained from the $1/(R_{gb}C_{gb})$ at different biases shown as open triangles in Fig. 6 agree perfectly with those deduced from the slope of Z' versus Z''/f. This indicates that the fitting equivalent circuit is suitable, which further convinces the conclusion that the resonance is related to an LC resonance and the relaxation is associated with the grain boundaries.

Based on the above results, we can now discuss the impedance spectra of the pure sample as shown in Fig. 7. Compared with the results of the BN-doped sample (Fig. 4), notable changes can be seen: First, the zero-bias semicircular arc is much larger than that of the doped sample indicating higher resistive grain boundaries in pure sample [Fig. 7(a)]. Second, apart from the low-frequency larger arc, a small hump is observable in the high-frequency range as clearly seen from the enlarged view of the terminal part shown in Fig. 7(b). This implies that there is another electric relaxation. In order to clarify the two relaxations, we resort to the use of dielectric modulus, M^*, which is defined as $M^* = j\omega C_0 Z^*$, where $\omega=2\pi f$ is the angular frequency, C_0 is the vacuum capacitance of the measuring cell. Figure 7(c) replots the impedance data in terms of the imaginary part of the dielectric modulus M'' as a function of frequency. This presentation was proved to be useful in separating two closed relaxations found in the presentation of Z'' versus Z'.[32] Indeed, two well separated peaks reflecting two dielectric relaxations in the new presentation can be seen. The possibility

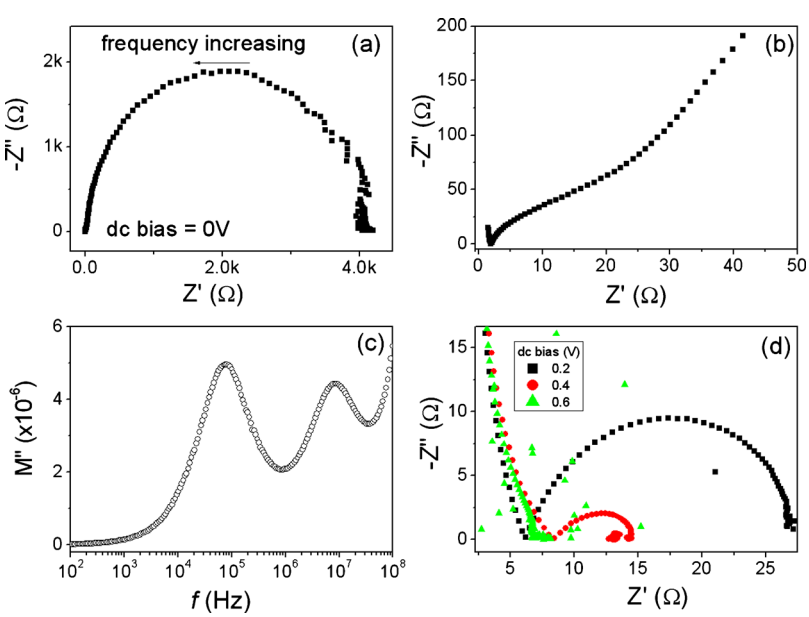

FIG. 7. (Color online) Complex impedance of pure sample. (a) Complex impedance at a dc bias of 0 V. (b) An enlarged view of the high-frequency part of Fig. 7(a) which clearly shows the resonance and another relaxation. (c) The same data in Fig. 7(a) were replotted in an alternative presentation in which modulus spectroscopic plots against frequency. (d) Complex impedance at various dc biases.

Downloaded 16 Aug 2012 to 130.130.37.84. Redistribution subject to AIP license or copyright; see http://jap.aip.org/about/rights_and_permissions

that the newly appeared relaxation is related to grains can be ruled out because it can be easily destroyed by dc bias as demonstrated in Fig. 7(d). For example, at the bias of 0.2 V, only one relaxation remains, while the bias increases to 0.6 V the remaining relaxation disappears completely. This fact indicates that the new polarization has a contribution from intergrains. Judging from the results of Fig. 1, the new relaxation might be ascribed to the contribution of MgO, since the pure sample has more pores than the doped sample, some grains are easily to be covered by insulating MgO layers resulting in the second polarization. While in the doped sample, MgO is effectively eliminated and hence only one relaxation can be detected. In short, the impedance analysis reveals an additional insulating layer alongside with the grain boundaries in the pure sample. The doping of the nano *h*-BN particles can effectively eliminate the insulating layer and hence improve the electric connectivity. This further convinces the conclusion in Sec. III A.

IV. CONCLUSIONS

In summary, we have performed a comparative investigation of pure and nano *h*-BN doped MgB_2 ceramics. We find that: (1) the addition of the nano *h*-BN can effectively eliminate MgO and pores resulting in a very high density and good connectivity of the doped sample. (2) The charge carriers in MgB_2 are free ones. This leads to the notable inductance effect of the measuring system and an *LC* resonance. (3) Two dielectric relaxations associated with the intergrains were detected in the pure sample and only one relaxation can be detected in the doped sample. This means that the addition of the *h*-BN can greatly reduce the intergrain resistivity, which in turn, improves the connectivity.

ACKNOWLEDGMENTS

The authors thank financial supported by Australian Research Council Discovery Grant (Grant No. DP0770205). L. Lu is thanked for sample preparation.

[1]J. Nagamatsu, N. Nakagawa, T. Muranaka, Y. Zenitana, and J. Akimitsu, Nature (London) **410**, 63 (2001).
[2]K. Vinod, R. G. A. Kumar, and U. Syamaprasad, Supercond. Sci. Technol. **20**, R1 (2007).
[3]X. X. Xi, Rep. Prog. Phys. **71**, 116501 (2008).
[4]M. Eisterer, Supercond. Sci. Technol. **20**, R47 (2007).
[5]E. W. Collings, M. D. Sumption, M. Bhatia, M. A. Susner, and S. D. Bohnenstiehl, Supercond. Sci. Technol. **21**, 103001 (2008).
[6]J. M. Rowell, Supercond. Sci. Technol. **16**, R17 (2003).
[7]J. M. Rowell, S. Y. Xu, X. H. Zeng, A. V. Pogrebnyakov, Q. Li, X. X. Xi, J. M. Redwing, W. Tian, and X. Pan, Appl. Phys. Lett. **83**, 102 (2003).
[8]A. Yamamoto, J. Shimoyama, K. Kishio, and T. Matsushita, Supercond. Sci. Technol. **20**, 658 (2007).
[9]M. Eisterer, J. Emhofer, S. Sorta, M. Zehetmayer, and H. W. Weber, Supercond. Sci. Technol. **22**, 034016 (2009).
[10]B. Ni, Y. Morita, Z. Liu, C. Liu, K. Himeki, E. S. Otabe, M. Kiuchi, and T. Matsushita, Physica C **468**, 1443 (2008).
[11]A. Polyanskii, V. Beilin, I. Felner, M. I. Tsindlekht, E. Yashchin, E. Dul'kin, E. Galstyan, M. Roth, B. Senkowicz, and E. Hellstrom, Supercond. Sci. Technol. **17**, 363 (2004).
[12]S. D. Kaushik and S. Patnaik, IEEE Trans. Appl. Supercond. **17**, 3016 (2007).
[13]X. G. Zheng, Y. Sakurai, Y. Okayama, T. Q. Yang, L. Y. Zhang, X. Yao, K. Nonaka, and C. N. Xu, J. Appl. Phys. **92**, 2703 (2002).
[14]C. C. Wang, Y. M. Cui, G. L. Xie, C. P. Chen, and L. W. Zhang, Phys. Rev. B **72**, 064513 (2005).
[15]A. Andreone, E. D. Gennaro, G. Lamura, M. Salluzzo, A. Purnell, L. F. Cohen, L. Hao, J. Gallop, C. Cantoni, and M. Paranthaman, Supercond. Sci. Technol. **16**, 260 (2003).
[16]C. E. Gough, R. J. Ormeno, A. Sibley, M. Hein, S. NishiZaki and Y. Maeno, J. Phys. Chem. Solids **63**, 2187 (2002).
[17]B. B. Jin, N. Klein, W. N. Kang, H. J. Kim, E. M. Choi, S. I. K. Lee, T. Dahm, and K. Maki, Supercond. Sci. Technol. **16**, 205 (2003).
[18]J. H. Jung, S. A. Seo, T. W. Noh, P. A. Sharma, N. Hur, and S. W. Cheong, Solid State Commun. **126**, 175 (2003).
[19]S. X. Dou, O. Shcherbakova, W. K. Yeoh, J. H. Kim, S. Soltanian, X. L. Wang, C. Senatore, R. Flukiger, M. Dhalle, O. Husnjak, and E. Babic, Phys. Rev. Lett. **98**, 097002 (2007).
[20]C. P. Bean, Rev. Mod. Phys. **36**, 31 (1964).
[21]R. H. T. Wilke, S. L. Bud'ko, P. C. Canfield, D. K. Finnemore, R. J. Suplinskas, and S. T. Hannahs, Physica C **424**, 1 (2005).
[22]P. Kováč, I. Hušek, T. Melišek, C. R. M. Grovenor, and S. Haigh, Supercond. Sci. Technol. **17**, 1225 (2004).
[23]J. Jiang, B. J. Senkowics, D. C. Larbalestier, and E. E. Hellstrom, Supercond. Sci. Technol. **19**, L33 (2006).
[24]D. Reagor, E. Ahrens, S. W. Cheong, A. Migliori, and Z. Fisk, Phys. Rev. Lett. **62**, 2048 (1989).
[25]E. A. Yelland, J. R. Cooper, A. Carrington, N. E. Hussey, P. J. Meeson, S. Lee, A. Yamamoto, and S. Tajima, Phys. Rev. Lett. **88**, 217002 (2002).
[26]Y. M. Cui, L. W. Zhang, and R. M. Wang, Physica C **442**, 29 (2006).
[27]C. C. Wang, M. He, F. Yang, J. Wen, G. Z. Liu, and H. B. Lu, Appl. Phys. Lett. **90**, 192904 (2007).
[28]J. C. C. Abrantes, J. A. Labrincha, and J. R. Frade, Mater. Res. Bull. **35**, 727 (2000).
[29]C. C. Wang, Y. M. Cui, and L. W. Zhang, Appl. Phys. Lett. **90**, 012904 (2007).
[30]C. C. Wang, G. Z. Liu, M. He, and H. B. Lu, Appl. Phys. Lett. **92**, 052905 (2008).
[31]W. Li and R. W. Schwartz, J. Am. Ceram. Soc. **90**, 3536 (2007).
[32]D. C. Sinclair and A. R. West, J. Appl. Phys. **66**, 3850 (1989).

Downloaded 16 Aug 2012 to 130.130.37.84. Redistribution subject to AIP license or copyright; see http://jap.aip.org/about/rights_and_permissions